JOURNAL OF MATERIALS SCIENCE **40** (2005) 1127–1134

Hydroxylapatite-zirconia composites: Thermal stability of phases and sinterability as related to the CaO-ZrO_2 phase diagram

Z. EVIS
Middle East Technical University, Engineering Sciences, Ankara, Turkey

C. ERGUN*
Istanbul Technical University, Mechanical Engineering, Taksim, Istanbul, Turkey
E-mail: ergunce@itu.edu.tr

R. H. DOREMUS
Rensselaer Polytechnic Institute, Materials Science and Engineering, Troy, NY 12180, USA

Composites of hydroxylapatite (HA) with pure zirconia, and 3 and 8% Y_2O_3 in zirconia, were pressure-less sintered at temperatures from 900 to 1300 °C, and hot-pressed at 1200 °C in argon gas atmosphere for 1 h. The reactions and transformations of phases were monitored with X-ray diffraction and thermal analysis. At sintering temperatures higher than 1000 °C, calcium from HA diffused into the zirconia phase, and the HA phase decomposed to tri-calcium phosphate (TCP). Above about 1200 °C, $CaZrO_3$ was formed. These reactions and transformations were interpreted in terms of the ZrO_2-CaO phase diagram. On the other hand, zirconia and hydroxylapatite phases in hot pressed composite remained mainly stable suggesting that air in the sintering environment increased the reactivity between the phases. The highest densification was found in a composite initially containing 10% monoclinic ZrO_2 sintered at 1300 °C. The densification of the composites decreased at lower sintering temperatures and higher zirconia contents upon air-sintering.

1. Introduction

Hydroxylapatite (HA, $Ca_{10}(PO_4)_6(OH)_2$), a kind of calcium phosphate type ceramic material [1, 2], is widely used in biomedical applications such as surgical [3] and dental implantology [4] because this material improves biocompatibility and bonds well to growing bone, since the chemical composition of HA is close to that of the inorganic component of bone. However, HA has some mechanical limitations because it is brittle. For this reason, HA-based composites or HA coatings on metals have been studied to enhance the mechanical properties of HA. For instance, composites made of HA and other ceramic powders [5–9], bioactive glasses [10] or polymers [11, 12] have been studied as candidate implant materials. HA-ceramic composites, especially HA-zirconia composites, have shown promising improvements in the strength and toughness as compared to HA itself [6, 7]. On the other hand, decomposition of HA, which forms second phases, and phase transformation of partially stabilized zirconia from tetragonal to cubic structure can degrade the mechanical properties of these composites [5, 6].

There have been many reports of processing of HA composites with zirconia [6, 9, 13–16]; many earlier references are reviewed in these papers. There is agreement that the addition of zirconia to the HA causes it to decompose at lower temperatures in pressure-less sintering, so that several workers have used hot-pressing to reach higher density [13–15].

The present study aimed to develop a more complete understanding of the thermal phase stability and interactions between hydroxylapatite and various zirconias and to investigate the sinterability of HA-zirconia composites, as interpreted with the ZrO_2-CaO phase diagram. Three types of zirconia; pure, 3 mol% yttria doped, 8 mol% yttria doped, were used to make HA composites. The composites were characterized with XRD, thermal analysis and sinterability in terms of density measurements.

2. Experimental procedures

HA was prepared by a precipitation method. Details on this technique are reported in a previous paper [17]. Zirconia powders were obtained from Zirconia Sales Inc. The particle diameter in our sintered composites was about 0.2 μm. The powders of HA and the ceramic components; (ZrO_2; 3 mol% Y_2O_3 doped ZrO_2; 8 mol%

*Author to whom all correspondence should be addressed.

TABLE I Abbreviation and the composition of the samples

Name	Abbreviation	Composition
Hydroxylapatite.	HA	pure
Zirconia.	ZrO_2	100%
3% mol.Y_2O_3 doped ZrO_2.	YSZ3	100%
8% mol.Y_2O_3 doped ZrO_2.	YSZ8	100%
Hydroxylapatite Zirconia Composites.	$HAZrO_2$-10	90 wt% HA+10 wt% ZrO_2
	$HAZrO_2$-25	75 wt% HA+25 wt% ZrO_2
	$HAZrO_2$-40	60 wt% HA+40 wt% ZrO_2
Hydroxylapatite- 3% mol.Y_2O_3 doped ZrO_2 Composites.	HAYSZ3-10	90 wt% HA+10 wt% YSZ3
	HAYSZ3-25	75 wt% HA+25 wt% YSZ3
	HAYSZ3-40	60 wt% HA+40 wt% YSZ8
Hydroxylapatite- 8% mol.Y_2O_3 doped ZrO_2Composites.	HAYSZ8-10	90 wt% HA+10 wt% YSZ8
	HAYSZ8-25	75 wt% HA+25 wt% YSZ8
	HAYSZ8-40	60 wt% HA+40 wt% YSZ8

Y_2O_3 doped ZrO_2) were mixed in the desired weight ratios. The description and the composition of the samples are shown in Table I. XRD measurements and thermal analysis for the phase analysis were performed just on the $HAZrO_2$-25 (75 wt% HA-25 wt% ZrO_2) composite samples. All composites were used for the sinterability measurements.

For homogeneous mixing, the powders were blended with ball milling in an ethyl alcohol medium. The milled powder was then quickly filtered through a 0.2 micron Millipore filter to prevent segregation due to the density differences of the two components. The filtered cakes were kept at 200 °C overnight to remove the rest of the ethyl alcohol. The cakes were crushed and further mixed in a pestle and mortar. The resulting powder was cold-pressed into pellets at 200 MPa in a cylindrical die. Subsequently, pellets were pressure-less sintered at 900, 1000, 1100, 1200, and 1300 °C for 1 h in air. XRD measurements and thermal analysis were only performed on the composites of $HAZrO_2$-25. Composite with this composition was also used for sintering with hot-pressing in argon at 1200 °C for 1 h to examine the effect of sintering environment on the phase stability of the components.

XRD analyses were performed on one of the surfaces of the sintered pellets with a Scintag XRD unit operating with Ni filtered Cu K_α radiation.

The densities of sintered cylindrical samples were calculated from their measured dimensions and weights. The theoretical density ρ_t of a composite sample of composition w_z wt% zirconia and w_h wt% HA was calculated from the formula:

$$\rho_t = \frac{1}{\frac{w_z}{5.89} + \frac{w_h}{3.156}} \quad (1)$$

in which 5.89 and 3.156 g/cm^3 are the densities of pure zirconia and HA, respectively. The fraction of the theoretical density (fractional density) is then just the measured density divided by ρ_t.

Thermal analyses were conducted to monitor reactions between HA and zirconia phases that occur during sintering. A TA Instruments SDT 2960 TGA system was used at 20 °C/min heating/cooling rate from room temperature to 1350 °C under 100 mL/min air purge for the analysis.

3. Results

Pure HA pellets were sintered in air for 1 h at temperatures of 900, 1000, 1100, 1200, and 1300 °C.

X-ray diffraction patterns showed slight decomposition of the HA only at 1300 °C. X-ray diffraction patterns of $HAZrO_2$-25 pellets sintered for 1 h at temperatures from 900 to 1300 °C are given in Fig. 1. As the sintering temperature increased the monoclinic ZrO_2 began to transform to tetragonal or cubic ZrO_2 at 1100 °C, and at 1200 °C the transformation was complete. HA started to decompose to a mixture of α and β tricalcium phosphate (TCP) at 1100 °C; at 1300 °C this decomposition was nearly complete, and the TCP was entirely α phase.

The more spread X-ray diffraction pattern in Fig. 2 for sample $HAZrO_2$-25 after 1 h at 1100 °C shows greater detail of the pattern of 2θ from 27° to 37°. The ZrO_2 was partially converted from monoclinic to tetragonal and/or cubic phases, and the HA has partially decomposed to TCP. Most of the diffraction lines for tetragonal and cubic ZrO_2 are close together; an example of the decomposition of the diffraction peaks near 2θ of 74° is shown in Fig. 3 for $HAZrO_2$-25 sintered at 1100 °C for 1 h in air. The zirconia is mainly tetragonal phase, with some cubic phase.

X-ray diffraction patterns of HAYSZ3-25 sintered in air at temperatures from 900° to 1300 °C are shown in Fig. 4, and for HAYSZ8-25 under the same conditions in Fig. 5. To compare the phases in the thee different composites containing ZrO_2, YSZ3 (3% Y_2O_3·ZrO_2),

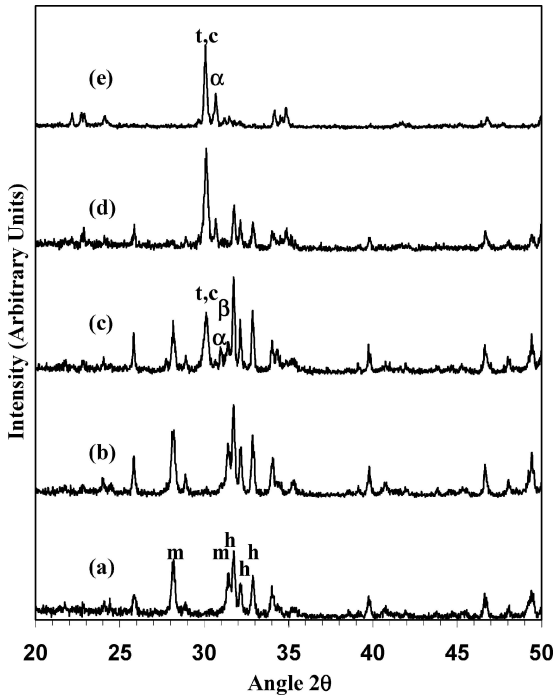

Figure 1 X-ray diffraction patterns of $HAZrO_2$-25 samples after sintering for 1 h in air at temperatures: (a) 900 °C, (b) 1000 °C, (c) 1100 °C, (d) 1200 °C, (e) 1300 °C. H are HA peaks; m, monoclinicZrO_2; t, c, tetragonal and/or cubic ZrO_2; α and β, tricalcium phosphate.

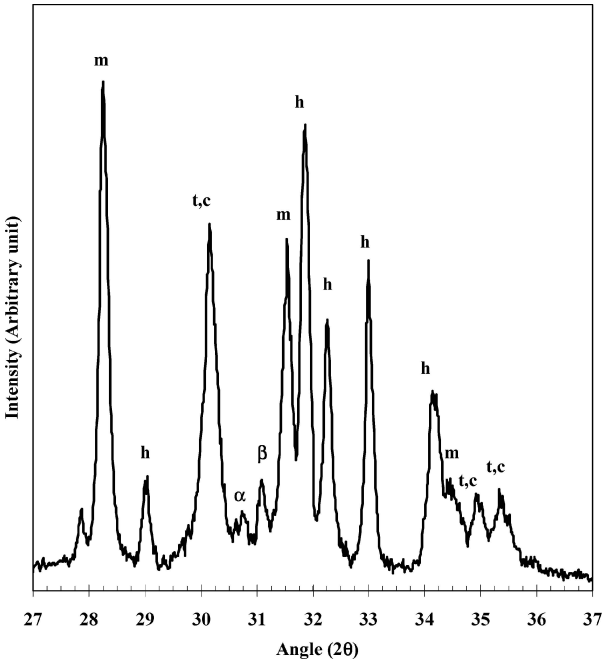

Figure 2 X-ray diffraction pattern of $HAZrO_2$-35 after sintering for 1 h in air at 1100 °C. h, hydroxylapatite; m, monoclinic ZrO_2; t, c, tetragonal and/or cubic ZrO_2; α, α-TCP, β, β-TCP.

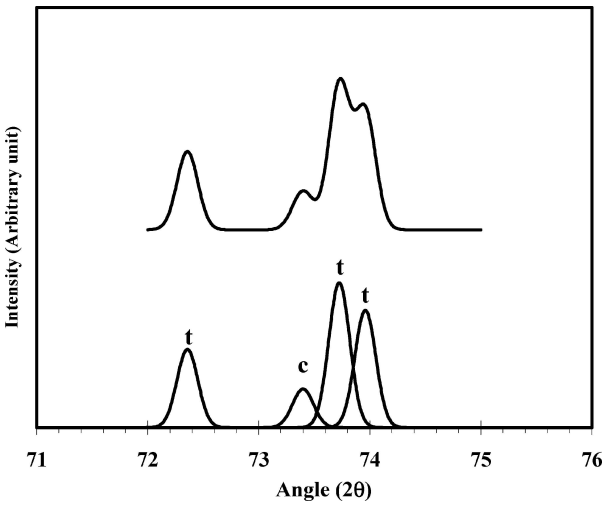

Figure 3 X-ray diffraction pattern for $HAZrO_2$-25 composite sintered for 1 h in air at 1100 °C. Top, measured curve, bottom decomposition of the main peak, *T*, tetragonal phase; *c*, cubic phase ZrO_2.

and YSZ8 (8% $Y_2O_3{\cdot}ZrO_3$) the relative XRD peak heights are plotted as a function of sintering temperatures in Figs 6–8. The relative peak heights show the changes in the amounts of a particular phase, but are not normalized to give absolute concentrations.

The decomposition reaction of HA as shown by the plots in Figs 6–8 to α and β TCP is:

$$Ca_{10}(PO_4)_6(OH)_2 \longrightarrow 3Ca_3(PO_4)_2 + CaO + H_2O \quad (2)$$

In Fig. 6 the HA peak shows that in composites with monoclinic ZrO_2 reaction 2 starts at between 900 and 1000 °C, and is almost complete between 1200 and 1300 °C. This behavior is much different than for pure HA, which started to decompose between 1200 and 1300 °C, Fig. 9. Thus the monoclinic ZrO_2 acts as a catalyst for the decomposition of HA. In Fig. 6 the monoclinic ZrO_2 begins to transform to tetragonal ZrO_2 at

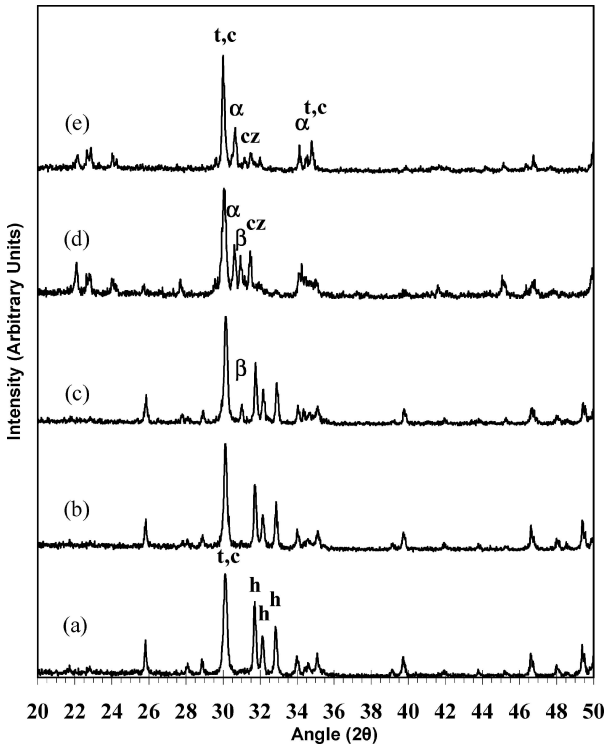

Figure 4 X-ray diffraction patterns for HAYSZ3-25 sintered in air for 1 h at (a) 900 °C, (b) 1000 °C, (c) 1100 °C, (d) 1200 °C, (e) 1300 °C. h, hydroxylapatite; t, c tetragonal and cubic ZrO_2; α, α-TCP; β, β-TCP; cz, $CaZrO_3$.

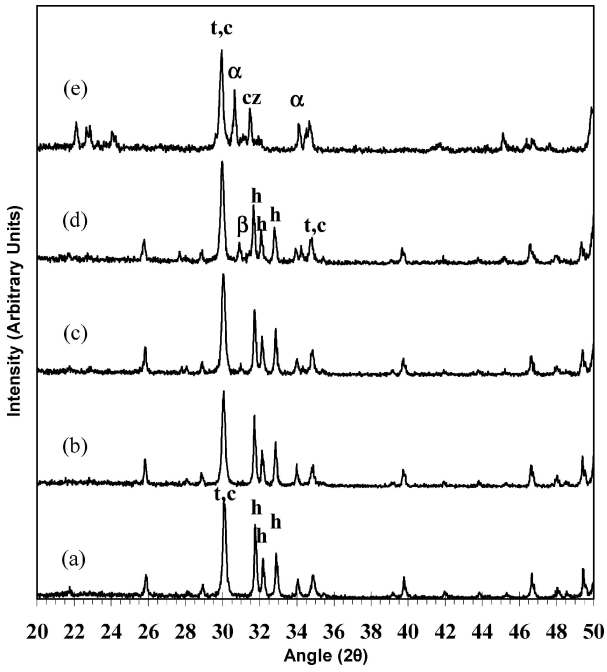

Figure 5 X-ray diffraction patterns for HAYSZ8-25 composites sintered in air for 1 h at (a) 900 °C, (b) 1000 °C, (c) 1100 °C, (d) 1200 °C, (e) 1300 °C. h, hydroxylapatite; t, c tetragonal and cubic ZrO_2; α, α-TCP; β, β-TCP; cz, $CaZrO_3$.

about 1000 °C, and is almost entirely transformed at 1200 °C suggesting that the transformation of monoclinic to tetragonal ZrO_2 is closely related to the decomposition of HA by reaction 2.

A comparison of HA curves in Figs 6 and 7 shows that when tetragonal YSZ3 ($3Y_2O_3{\cdot}97ZrO_2$) is substituted for monoclinic ZrO_2 in the 25% ZrO_2 composites, the decomposition of HA is retarded, and

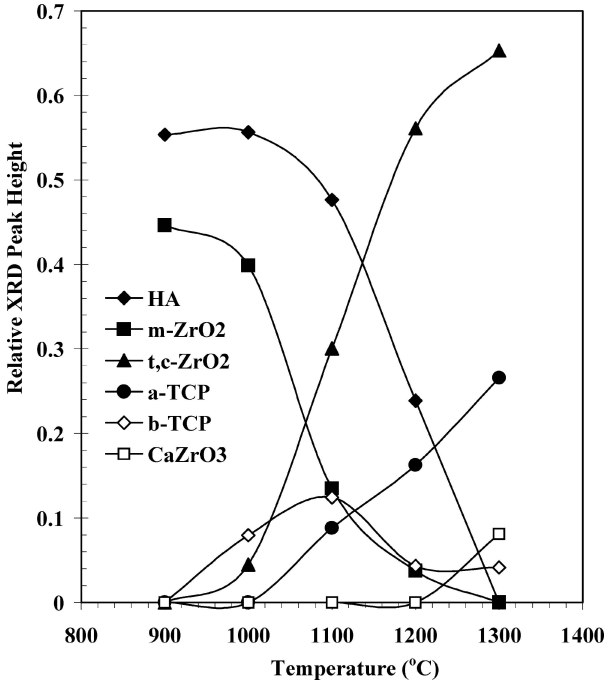

Figure 6 Relative amounts of different phases in $HAZrO_2$-25 composites sintered at different temperatures, from peak heights in Fig. 1.

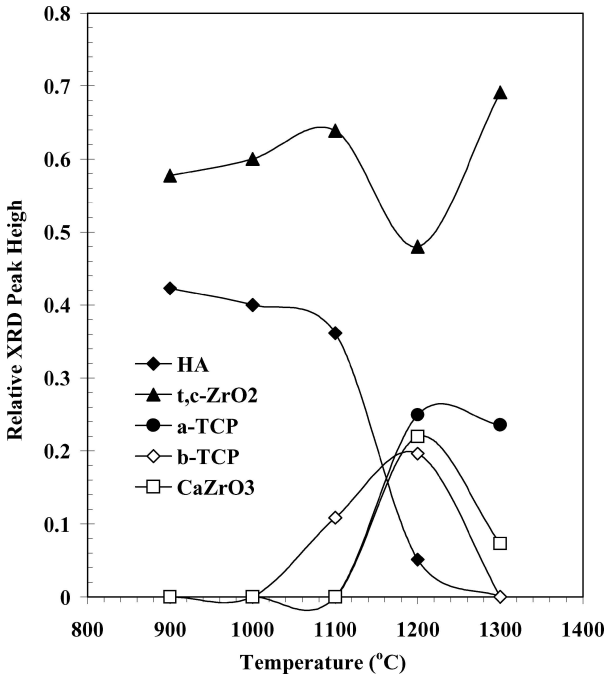

Figure 7 Relative amounts if different phases in HAYSZ3-25 composites after sintering for 1 h at different temperatures, from the peak heights in Fig. 4.

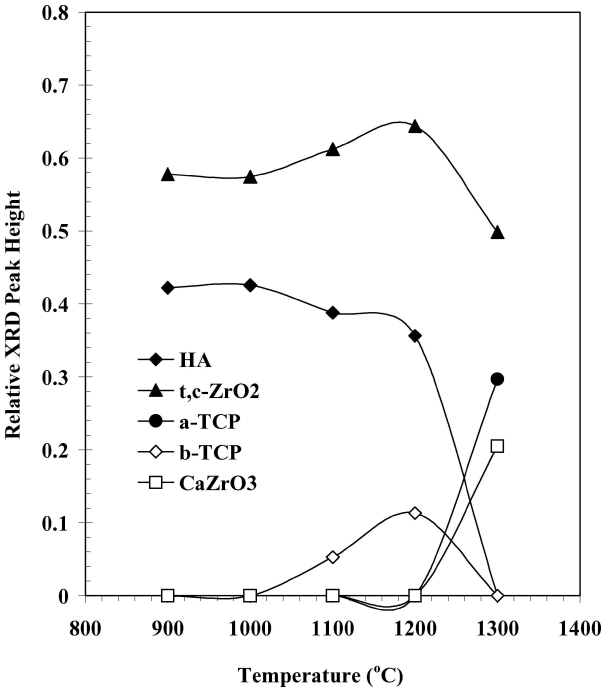

Figure 8 Relative amounts of different phases in HAYSZ8-25 composites after sintering for 1 h at different temperatures, from the peak heights in Fig. 5.

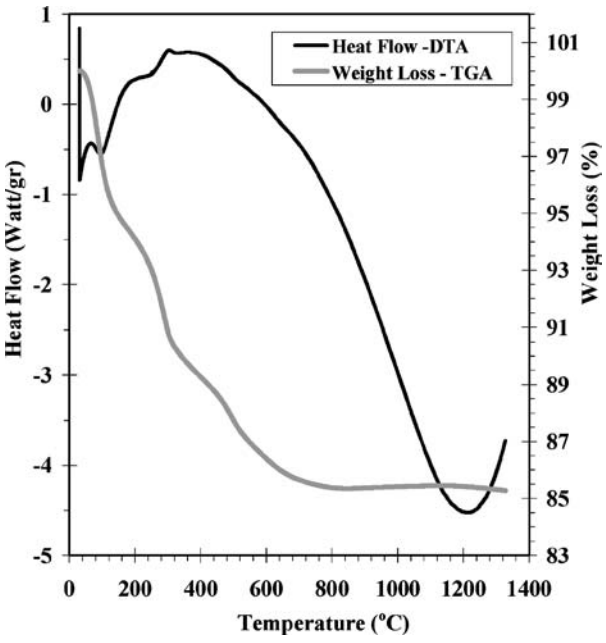

Figure 9 TGA and DTA of HA up to 1300 °C.

starts at between 1000 and 1100 °C instead of under 1000 °C. With 25% YSZ8 ($8Y_2O_3{\cdot}92ZrO_2$) in the HA composites (Fig. 8) the decomposition of HA starts also between 1000 and 1100 °C, however the first appearance of $CaZrO_3$ was between 1200 and 1300 °C instead of at lower temperatures in composites with the other zirconias. In HA-ZrO2 composites, the HA phase almost completely disappeared.

As the relative amounts of α and β-TCP can also be followed from the plots in Fig. 6, β-TCP phase forms first from reaction 2 between 900 and 1000 °C, and α-TCP first appears between 1000 and 1100 °C; both phase are observed in the composite sintered at 1300 °C. However in Figs 7 and 8 for the composites of HAYSZ3-25 and HAYSZ8-25, β-TCP phase forms first from reaction 2 between 1000 and 1100 °C, and α-TCP first appears between 1100 and 1200 °C in Fig. 7 for HAYSZ3-25, and 1200 and 1300 °C in Fig. 8 for HAYSZ8-25 and completely disappeared at 1300 °C.

Formation of $CaZrO_3$ was monitored in Figs 6, 7 and 8 between 1200 and 1300 °C. The CaO formed by the decomposition of HA (reaction 2) can react with zirconia to form $CaZrO_3$ according to the following reaction:

$$CaO + ZrO_2 \longrightarrow CaZrO_3 \qquad (3)$$

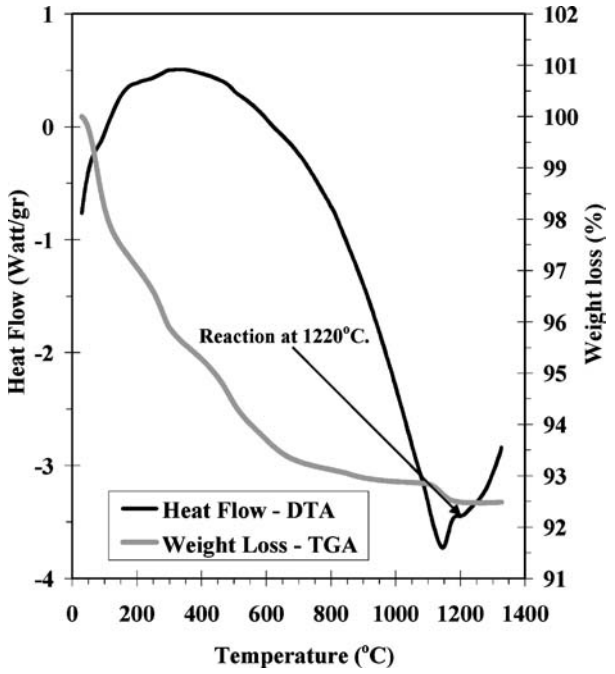

Figure 10 TGA and DTA of $HAZrO_2$-25 up to 1300 °C.

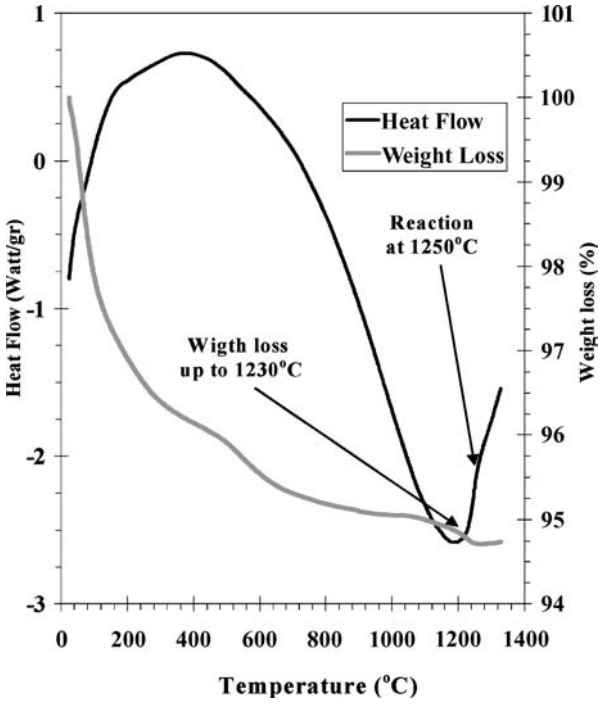

Figure 11 TGA and DTA of HAYSZ3-25 up to 1300 °C

Thermogravimetric analysis (TGA) of pure HA, Fig. 9, showed a continuous weight loss of about 5% from room temperature to about 700 °C, which probably results from removal of absorbed molecular water and combination of surface OH groups on the apatite to form water. At 1200 °C in differential thermal analysis (DTA) there was an endothermic peak at about 1200 °C, which probably resulted from the beginning of HA decomposition. The TGA curve for $HAZrO_2$-25 composite in Fig. 10 shows the weight loss from absorbed water up to about 600 °C, just as found for pure HA. The additional weight loss at about 1200 °C probably results from the decomposition of HA by reaction 2. The endothermic DTA peak at about 1220 °C is attributed to the formation of $CaZrO_3$ by reaction 3. The TGA curve for HAYSZ3-25 composite in Fig. 11 also showed the same weight loss trend similar to pure HA. However, the heel of the TGA curve indicating the weight loss was extended to 1260 °C, which was up to 1160 °C in the $HAZrO_2$-25 in Fig. 10.

The X-ray diffraction pattern for $HAZrO_2$-25 composite hot-pressed in argon at 1200 °C for 1 h, Fig. 12, showed lesser decomposition of HA than for the sample pressure-less sintered at the same time and temperature (Fig. 1d). Furthermore, the monoclinic zirconia phase in the pressure-less sintered sample had completely transformed to tetragonal ZrO_2 at 1200 °C, whereas the ZrO_2 in the hot-pressed sample was only partially transformed to tetragonal phase.

The % theoretical density is shown in Figs 13, 14 and 15 as a function of ZrO_2 content for composites sintered for 1 h at different temperatures. A maximum in density was found for a composite initially containing 10% monoclinic ZrO_2 and sintered at 1300 °C for 1 h; however, this composite contains little HA, which had been almost entirely converted to TCP by reaction 2 (Figs 1 and 6). Composites containing more than 20% ZrO_2, either pure or with Y_2O_3, had much lower densities.

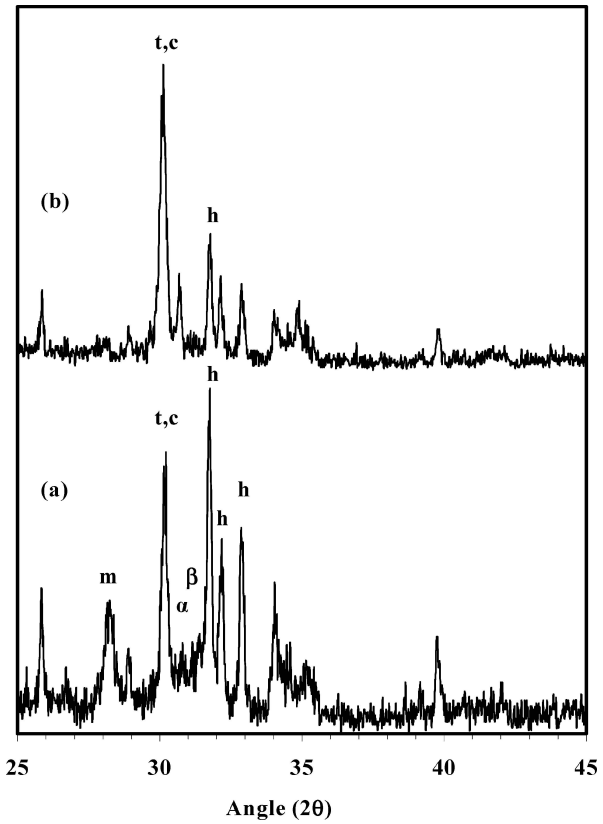

Figure 12 XRD patterns of $HAZrO_2$-25 composites: (a) hot-pressed in Ar atmosphere at 1200 °C for 2 h and (b) sintered in air for 2 h. *h* are HA peaks; m, monoclinic ZrO_2; t, c, tetragonal and/or cubic ZrO_2; α, tricalcium phosphate.

The densities of composites containing YSZ8, Fig. 14, were similar to these containing YSZ3 in Fig. 13.

4. Discussion

The chemical reactions of decomposition of HA (Equation 2) and formation of $CaZrO_3$ (Equation 3), as well

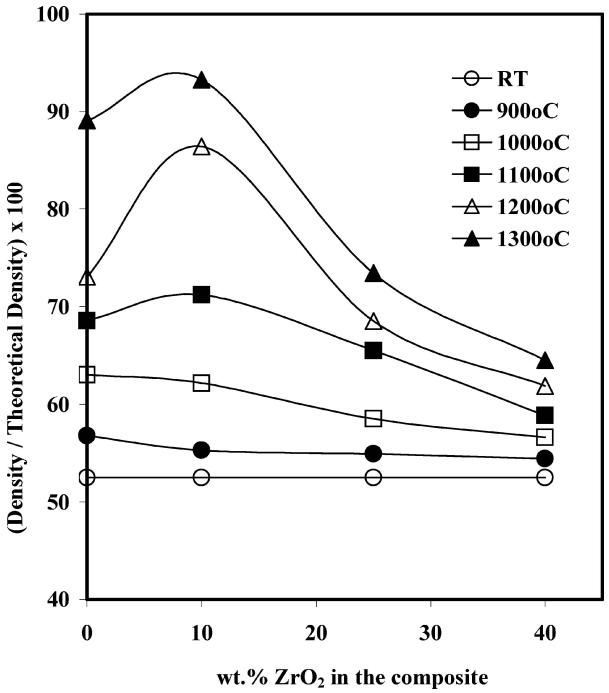

Figure 13 (Density/theoretical density) ×100 as a function of amount of monoclinic ZrO_2 in $HAZrO_2$ composites, after sintering for 1 h at different temperatures. Theoretical density from Equation 1.

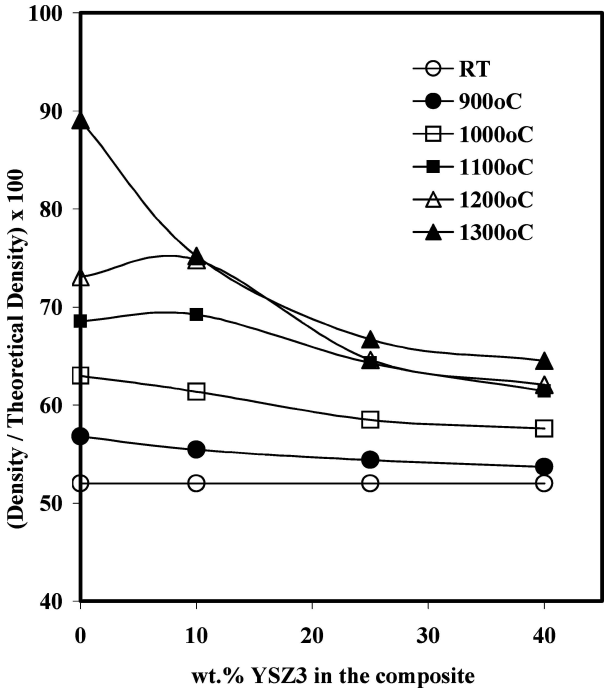

Figure 14 (Density/theoretical density) ×100 as a function of amount of YSZ3 ($3\%Y_2O_3{\cdot}97\%ZrO_2$) in HA-$ZrO_2$ composites sintered for 1 h at different temperatures.

as the transformation of zirconia phases, can be discussed in terms of the phase diagrams of ZrO_2-CaO and ZrO_2-Y_2O_3. ZrO_2-CaO in Ref. [18], Ref. [19], and Ref. [20]. These diagrams agree that pure monoclinic ZrO_2 is stable up to about 1200 °C, where it transforms to the tetragonal phase.

In the following discussion we have chosen the $ZrO_2{\cdot}CaO$ diagram from Ref. 19 and the $ZrO_2{\cdot}Y_2O_3$ diagram from Ref. 20 as the most reliable; see Ref. 18 for discussion of these diagrams and others.

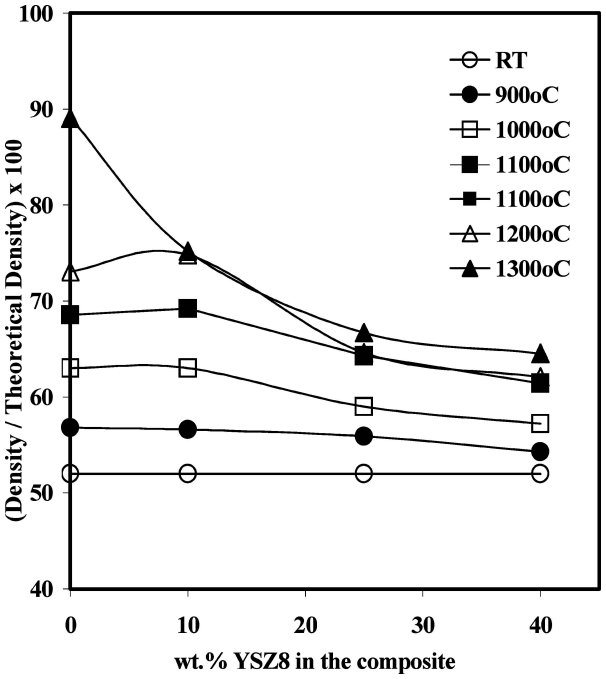

Figure 15 (Density/theoretical density) ×100 as a function of amount of YSZ8 ($8\%Y_2O_3{\cdot}97\%ZrO_2$) in HA-$ZrO_2$ composites sintered for 1 h at different temperatures.

In the composites containing pure monoclinic ZrO_2 and HA, the ZrO_2 begins to transform to tetragonal ZrO_2 at 1000 °C (Figs 1 and 6). This result is contrary to the phase diagram in Ref. [19], in which tetragonal ZrO_2 is stable only above 1048 °C. At 1100 °C from this diagram there is a mixture of monoclinic and tetragonal ZrO_2 in the composition range of about 0.5 mol% CaO to 1.2 mol% CaO; above 1.2 mol% CaO the stable phase is tetragonal solid solution to 9.3 mol% CaO. At 1100 °C there is a region of mixed tetragonal and cubic ZrO_2 phases from CaO concentration of about 9.3 mol% to 17.2 mol%, and a small region of single-phase cubic ZrO_2 from about 17.2% to 17.5 mol% CaO. Thus the effective solubility of CaO in ZrO_2 at 1100 °C is about 17.5 mol%.

The diffusion of CaO into the ZrO_2 grains from the apatite can be visualized schematically, as shown in Fig. 14, based on these phase boundaries. It is assumed that phase equilibrium is reached rapidly at 1100 °C; metastable phases are unlikely but possible. The maximum CaO solubility at the ZrO_2 surface is 17.5 mol%, forming a thin region of single-phase cubic ZrO_2; the regions II–V in Fig. 14 then follow from the phase boundaries. The mixture of phases shown in Figs 1, 2, 3 and 6 is consistent with this schematic picture of successive phase transformations in the zirconia; at 1100 °C the majority phase is tetragonal ZrO_2, with lesser amounts of cubic (Fig. 3) and monoclinic ZrO_2.

After 1 h at 1200 °C there is still some monoclinic ZrO_2 in the $HAZrO_2$-25 composite, suggesting that the temperature needed to transform monoclinic phase to tetragonal is actually somewhat higher than 1200 °C. After 1 h at 1300 °C, there was no monoclinic ZrO_2 remaining.

An approximate diffusion coefficient of CaO in the zirconia particles can be estimated from the mean size

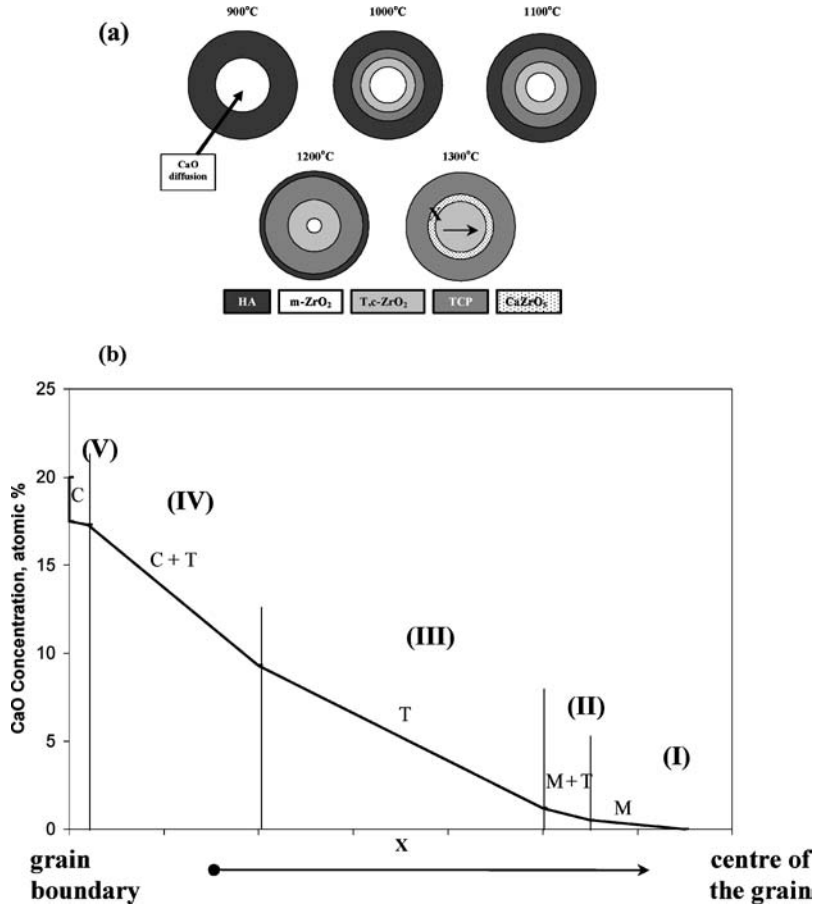

Figure 16 (a) Phase distribution around a zirconia grain with increasing sintering temperatures (between 900 and 1300°C), (b) Schematic diagram of the profile of CaO diffusing into a grain of initially monoclinic zirconia (M). As the CaO concentration increases, the zirconia transforms to tetragonal (t) and cubic (c) phases. X is the distance from the ZrO_2-HA interface.

of these particles (about 0.1 μm in diameter). Then from the Einstein formula

$$D = \frac{x^2}{2t} \tag{4}$$

in which x is the mean diffusion distance (roughly the particle radius of 0.05 μm), t the diffusion time of 1 h, and D the diffusion coefficient , $D \approx 6(10)^{-15}$ cm^2/s at 1100 °C.

As more CaO becomes available from decomposition of HA, $CaZrO_3$ forms by reaction 3. The Gibbs free energy of this reaction at 1300 °C is about—54 kJ/mole, so it is quite favorable. At 1220 °C, $CaZrO_3$ begins to form in the $HAZrO_2$-25 composites (Fig. 4), presumably on the surfaces of the tetragonal and cubic ZrO_2 particles. After the CaO concentration thoughout the ZrO_2 particles has reached the saturation solubility, any additional CaO should be consumed to form $CaZrO_3$ by reaction 3.

When the starting zirconia powder contains 3 or 8 mol% Y_2O_3, it is in the tetragonal and cubic structures, with no monoclinic ZrO_2 phase present (Figs 7 and 8). This powder is less reactive with CaO at 1100 °C than the pure monoclinic ZrO_2, leading to a lower decomposition of HA in the composite at this temperature. Perhaps the reason for this lower reactivity is that the diffusion of CaO in the ZrO_2 containing some Y_2O_3 is slower than in the ZrO_2 without Y_2O_3, because the ternary ZrO_2·Y_2O_3·CaO diagram shows no evidence for any reduction of CaO solubility when Y_2O_3 is present (ref. 18 diagram). Thus the effect of Y_2O_3 is apparently to reduce the diffusion coefficient of CaO in the ZrO_2. One can speculate that some of the defects involved in diffusion are taken up by the Y_2O_3, leaving fewer defects for diffusion of CaO. The $CaZrO_3$ begins to form at 1220 °C with the ZrO_2, containing Y_2O_3 instead of at 1300 °C as for the composites starting with pure ZrO_2, probably because of greater build-up of CaO at the ZrO_2 surface as a result of slower CaO diffusion in the ZrO_2.

In the hot-pressed HAYSZ3-25 the hydroxylapatite and zirconia phases stayed mainly stable after sintering in the inert Ar gas environment; suggesting that the presence of air presumably oxygen in the sintering environment increased the reactivity between the 2 phases leading to faster decomposition of HA into TCP in the existence of zirconia, and then the released CaO was latter consumed by diffusing into the monoclinic zirconia causing its phase transformations to tetragonal/cubic phase.

The density measurements for the sinterability evaluations of the composites showed that the $HAZrO_2$-10 (10% monoclinic ZrO_2) composite sintered at 1300 °C (Fig. 11) had the highest density. Sintering at lower temperatures or higher ZrO_2 contents caused lower densification. When the starting powder is ZrO_2 with 3 or 8 mol% Y_2O_3, the densification is much lower after sintering the composite containing 10% ZrO_2 (Fig. 12)

at 1200 or 1300 °C; the reason for this difference is not clear, because the decomposition of HA is about the same for all the composites at these temperatures (Figs 7–10). Other factors in addition to the decomposition of HA are apparently influencing the porosity.

When hot–pressing at 1200 °C for 1 h is employed for sintering of HAYSZ-25 composites; the densification was considerably increased yielding to about 99% of its theoretical density, perhaps because of higher gas (water vapor?) pressure in the pores, and faster diffusion out of the pores.

Since the zirconia reinforcement is used to improve the mechanical properties of HA for possible load bearing implant applications, porosity may not be appreciated due to its strength decrement effects. However, more experiments are needed to evaluate the strength-porosity characteristics of these composites for possible applications where proper strength combining with porosity is demanded for the implant applications with a better incorporation with biological tissue [21].

References

1. T. S. B. NARASARAJU and D. E. PHEBE, *J. Mater. Sci.* **31** (1996) 1.
2. R. H. DOREMUS, *ibid.* **27**(2) (1992) 285.
3. T. MOILANEN, G. W. STOCKS, M. A. R. FREEMAN, G. SCOTT, W. D. GOODIER and S. J. W. EVANS, *J. Bone and Joint Surgery* **78-B** (1996) 200.
4. J. C. TAYLOR, C. F. DRISCOLL and M. D. CUNNINGHAM, *J. Prosthetic Dentistry* **75** (1996) 353.
5. M. TAKAGI, M. MOCHIDA, N. UCHIDA, K. SAITO and K. UEMATSU, *J. Mater. Sci. Mater. Med.* **3** (1992) 199.
6. J. M. WU and T. S. YEH, *J. Mater. Sci.* **23** (1998) 3777.
7. C. ERGUN and R. H. DOREMUS, *Turkish J. Engng. Environ. Sci.* **23** (2003) 485.
8. J. LI, B. FARTASH and L. HERMANSSON, *Biomaterials* **12** (1991) 438.
9. W. PYDA, A. SLOSARCZYK, M. HABERKO, Z. PASZKIEWICZ, A. RAPACZ-KMITA and A. PYDA, *Key Engng. Mater.* **206–213** (2002) 1567.
10. K. DOREMUS KANGASNIEMI, K. DEGROOT, J. WOLKE, O. ANDERSSON, Z. LUKLINSKA, J. G. M. BENCHT, M. LAKKISTO and A. YLI-URPO, *J. Mater. Sci. Mater Med.* **2** (1991) 133.
11. S. DEB, M. WANG, K. E. TANNER and W. BONFIELD, *ibid.* **7** (1996) 191.
12. R. LABELLA, M. BRADEN and S. DEB, *Biomaterials* **15** (1994) 1197.
13. J. ZI, H. ZIAO and L. H. HERMANSSON, *ibid.* **17** (1996) 1787.
14. E. ADOLFSSON, P. ALBERIUS-HENNING and L. HERMANSSON, *J. Amer. Ceram. Soc.* **83**(11) (2000) 2798.
15. V. V. SILVA, F. S. LAMEIRAS and R. Z. DOMINGUES, *Comp. Sci. Tech.* **61** (2001) 301.
16. R. R. RAE and T. S. KANNAN, *Mater. Sci. Eng.* **C20** (2002) 187.
17. C. ERGUN, T. J. WEBSTER, R. BIZIOS and R. H. DOREMUS, *J. Biomed. Mater. Res.* **59**(2) (2002) 312.
18. R. S. ROTH, "Phase Equilibrium Diagrams" (Am. Ceramic Soc., Westerville, OH, 43081) Vols. XI and XII.
19. P. DURAN, P. RECIO and J. RODRIGUEZ, *Mat. Sci.* **22** (1987) 4348.
20. R. RUH, K. S. MAZDIYAMI, P. G. VALENTINE and N. O. BIELSTEIN, *J. Amer. Ceramic Soc.* **67** (1984) C190.
21. Z. ZYMAN, V. GLUSHKO, V. FLIPPENKON, V. RADCHENKO and V. MEZENTSEV, *J. Mater. Sci: Mater. Med.* **15** (2004) 551.

Received 3 September
and accepted 1 November 2004